Hindawi
Geofluids
Volume 2020, Article ID 8836349, 8 pages
https://doi.org/10.1155/2020/8836349

Research Article

Permeability Characteristics of Coal after Supercritical CO_2 Adsorption at Different Temperatures

Xueying Liu,[1,2] **Jin Yu**,[1] **Di Wu**,[2] **and Xiaochun Xiao**[2]

[1]*Fujian Research Center for Tunneling and Urban Underground Space Engineering, Huaqiao University, Xiamen 361021, China*
[2]*School of Mechanics and Engineering, Liaoning Technical University, Fuxin, Liaoning 123000, China*

Correspondence should be addressed to Jin Yu; bugyu0717@163.com

Received 9 July 2020; Revised 3 August 2020; Accepted 27 August 2020; Published 9 September 2020

Academic Editor: Stefan Iglauer

CO_2 storage in coal seams has become one effective method to reduce CO_2 emission and help exploit coalbed methane (CBM). The permeability is a key parameter for CBM extraction. In deep coal seams (>800 m), CO_2 exists in the supercritical state. In the present work, permeability tests were performed on briquettes before and after supercritical CO_2 (SC-CO_2) adsorption at various temperatures to investigate the effects of SC-CO_2 adsorption on the permeability. Experimental results show that SC-CO_2 adsorption leads to volumetric expansion and permeability augment. The permeability enhancement decreases continuously at 35°C, while it initially increases and reduces at pressures exceeding 9 or 10 MPa at 45 or 55°C, respectively. Besides, the permeability enhancement ratio shows a linear increase with the expansion. The research provides a basis for further research on the enhanced coalbed methane (ECBM) recovery.

1. Introduction

The emission of CO_2 has been increasing over the years, and carbon capture and storage (CCS) has been considered to mitigate greenhouse effects [1]. Among various storage options (oil reservoirs, saline aquifers, and coal seams), storage in coal seams is promising because of advantages: firstly, there are plenty of unmineable coal resources because of limited recovery, and potential reserves of CBM in China ranks third in the world [2]; secondly, due to greater affinity of CO_2 to coal than CH_4, it contributes to ECBM recovery. Researchers from America, Japan, and China have performed pilot experiments for ECBM feasibility [3–5]. Specifically, when the temperatures and pore pressures are above the critical point (31.06°C, 7.38 MPa), CO_2 exists in a supercritical state in coal seams with a depth under 800 m [6]. SC-CO_2 has the characteristics of strong diffusion, low viscosity, and surface tension.

Research has been carried out on ECBM through experiments and numerical simulations [7–10]. When CO_2 is pressurized into coal seams, gas transport mainly includes diffusion, seepage, and competitive adsorption [11]. Adsorption of CO_2 has been investigated from the subcritical state to the supercritical state [12, 13], and various adsorption models have been assessed, such as Langmuir, Dubinin-Astakhov (D-A), and Dubinin-Radushkevich (D-R) models [14]. The adsorption could induce swelling [15, 16] and change the pore distribution, surface area, and function groups of coal [17, 18], leading to the variation in the seepage characteristics and mechanical properties [19, 20]. Pores are classified as micropores (<2 nm) for adsorption, mesopores (2-50 nm), and macropores (>50 nm) for seepage, and changes in pore structures have been investigated to reveal the mechanism. Sampath et al. compared the effects of short-term and long-term CO_2 interaction on pore structures [21]. Considered the existence of water in coal seams, Ni et al. [22] and Liu et al. [23] investigated the interaction with SC-CO_2 and water, indicating that the chemical reaction also influences pore structures.

The permeability is a key parameter for gas exploitation, and it is influenced by the effective stress and CO_2 adsorption, occasionally along with extraction and dissolution. Although previous studies have focused on permeability variation, however, the specific influence of each factor is uncertain, especially in the supercritical state. In the present

work, a series of permeability tests were performed before and after SC-CO_2 adsorption under nonconfining conditions at different temperatures. The effect of CO_2 adsorption on the permeability is investigated, and porosity differences between specimens are reduced by using briquettes. Results can provide a basis for further field application of ECBM.

2. Experimental Specimens and Apparatus

2.1. Specimens. The porosity of specimens drilled from the same block may be different, and this difference can influence the permeability characteristics and adsorption capacity. Therefore, the briquettes are selected as the specimens because of homogeneity and controllable porosity.

Blocks are extracted from Xinqiu Mine, Fuxin, Liaoning Province. The blocks are crushed and sieved until the diameter is below 0.25 mm. 255 g pulverized coal and 5 g rosin are put together into a cylinder with a thick wall, and a briquette is shaped in the cylinder with a loading of 460 kN as shown in Figure 1. The diameter and length are 50 mm and 100 mm, respectively. All specimens are dried at the temperature of 105°C for 24 hours. The average porosity is 0.31 by comparing the apparent density of specimens and the true density of powdered coal, and it can be considered that there is no difference between specimens.

2.2. Experimental System. The experiments include two parts, permeability tests and adsorption experiments. Based on Darcy's law, transient and steady-state methods are frequently used to determine permeability [24–26]. In the present work, the latter method is used because of the relatively high permeability of briquettes. The experimental system for permeability tests consists of the injection part (N_2 cylinder), a seepage and reference cell, a pump with a regulator, and a flow meter as shown in Figure 2. After being vacuumed, confining pressures are applied by the pump firstly. N_2 is pressured into the reference cell, and once the pressure is stable, N_2 is injected into the seepage cell to start the test. The flow meter is used to measure the flow rate of N_2, and the permeability is determined by [27]

$$k = \frac{2\mu P_2 LQ}{\left(P_1^2 - P_2^2\right)A}, \quad (1)$$

where μ is the viscosity of N_2, Q is the flow rate. P_1 and P_2 are the upstream and downstream pressures, respectively, and L and A are the length and cross-sectional area, respectively.

The main parts of the experimental system for adsorption are the reference cell and adsorption cell. The adsorption amount is measured by the volumetric method, and the void volume is estimated by injecting He according to the national standard. The diameter and length of a specimen at several positions are measured with a vernier caliper to calculate the volume before and after the experiment, and volumetric expansion can be determined by

$$S = \frac{(V - V_0)}{V_0} \times 100\%, \quad (2)$$

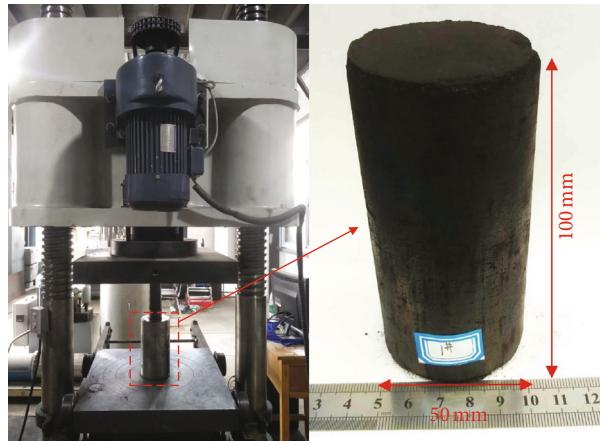

(a) (b)

Figure 1: The process of making a specimen.

where S is volumetric swelling and V_0 and V are the initial and final volume of the specimen, respectively.

According to the measurement in Wu et al. [13], the adsorption amount can be determined by

$$n = \frac{1}{mRT}\left[V_R\left(\frac{P_{R1}}{Z_{R1}} - \frac{P_{R2}}{Z_{R2}}\right) - \left(\frac{V_{A1}P_{A1}}{Z_{A1}} - \frac{V_{A2}P_{A2}}{Z_{A2}}\right)\right], \quad (3)$$

where n is the excessive adsorption amount per unit of a specimen. m is the weight of a specimen. R, the universal gas constant, is 8.314 J/(g·mol·K). T is the equilibrium temperature. V_R and V_A are the void volumes of reference and adsorption cells, and P_R and P_A are respective pressures of two cells. Subscripts 1 and 2 refer to the initial and final state, respectively. Z_{R1}, Z_{R2}, Z_{A1}, and Z_{A2} are compressibility factors corresponding to P_{R1}, P_{R2}, P_{A1}, and P_{A2}, respectively, at the temperature of T.

2.3. Experimental Procedures. The experimental procedures cover three stages, determining the permeability, CO_2 adsorption, and measuring the permeability after CO_2 desorption.

Stage one: a series of permeability tests are performed on a briquette placed in the seepage cell using N_2 with the injection pressure of 2 MPa and confining pressure of 12 MPa at 35°C

Stage two: the specimen is taken out from the seepage cell and placed in the adsorption cell. Experiments of CO_2 adsorption are conducted without confinement at the pressure of 8 MPa and temperature of 35°C. The experiment lasts for 24 hours according to the national standard, and the pressure reduction and deformation are recorded

Stage three: after desorption for 12 hours, permeability tests are repeated three times to investigate the variation and determine the effect of adsorption on the permeability.

A new specimen is replaced in the adsorption cell, and the second and third stages are repeated at CO_2 pressures of 9, 10, 11, 12, and 13 MPa. Subsequently, the temperature is increased to 45 or 55°C; this series of experiments are repeated.

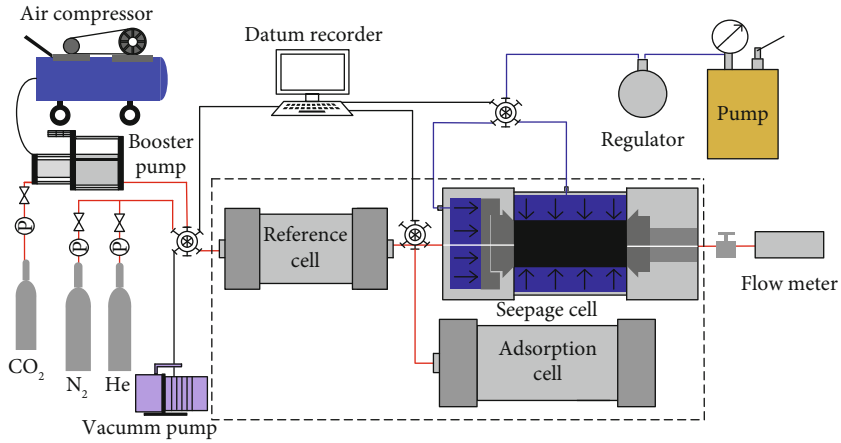

Figure 2: Experimental system.

3. Experimental Results and Discussion

3.1. Permeability Characteristics before and after SC-CO_2 Adsorption. Figure 3 shows that the permeability enhances remarkably after SC-CO_2 adsorption at different temperatures. After the adsorption, the permeability decreases by 0.4 mD with pressures ranging from 8 MPa to 9 MPa, and it reduces by approximately 0.7 mD at pressures increasing from 9 MPa to 13 MPa at 35°C. Nevertheless, the permeability after CO_2 adsorption increases slightly initially and subsequently decreases moderately with the increase of CO_2 pressures at 45 and 55°C, and peaks are observed obviously at the pressures of 9 MPa at 45°C. Compared with the initial permeability, the permeability enhancement ratio, η, can be determined by

$$\eta = \frac{(k - k_0)}{k_0} \times 100\%, \tag{4}$$

where k_0 and k are permeability values before and after CO_2 adsorption, respectively.

To reveal the variation of η with temperatures, the ratio is replotted as shown in Figure 4. The ratio decreases by approximately 13% at the pressure of 8 MPa, while it increases by 10% before decreasing at 9 MPa. When pressures are in the range of 10-13 MPa, the proportion increases slightly with temperatures ranging from 35 to 45°C, and it continues rising moderately with the increase of temperatures to 55°C.

3.2. Adsorption and Deformation. Figure 5 demonstrates that CO_2 adsorption induces various swelling at different pressures and temperatures. The volumetric swelling reduces by 4% at 35°C, while the expansion increases slightly before 9 MPa and subsequently decreases by 3.5% and 1.2% at 45 and 55°C, respectively. When pressures exceed 10 MPa, the expansion at 55°C is greater than that at other temperatures.

Although the Langmuir model is generally applied to estimate the adsorption amount and deformation, however, it is poorly applied to adsorption at pressures exceeding 6 MPa mainly due to the assumption of monolayer adsorption. Alternatives such as the modified D-R model have been found more suitable to fit with the adsorption amount and swelling [28, 29]. In this model, gas densities replace the pressures and adsorbed densities replace the saturated vapor pressures, which avoids the limitation of saturated vapor pressure in the supercritical state, as shown in

$$S = S_{\max} \exp\left(-D \ln^2 \frac{\rho_a}{\rho}\right) + a\rho, \tag{5}$$

where $S_{\max}$ is the maximum swelling. For adsorption amount, D is related to the adsorption heat and affinity of the gas to the sorbent, while for swelling it is possibly regarded as an empirical parameter. ρ, CO_2 density, varies with temperatures and pressures and is obtained from the website of the US National Institute of Standards and Technology (NIST), as shown in Figure 6. ρ_a, the density of the adsorbed phase, is considered as 1000 kg/m^3 [28, 29].

The deformations of specimens at three temperatures are fitted with the modified D-R model with a great determination as shown in Figure 7 and Table 1. $S_{\max}$ decreases by 13% with temperatures ranging from 35 to 55°C, while it does not vary significantly with the temperatures in the previous study [29]. This difference is mainly because the briquette structure is loose, while the structure of raw coal specimens is dense. The adsorbed density of CO_2 is approximately close to liquid CO_2 density, revealing that the adsorbed CO_2 requires less volume than gaseous CO_2. The a term is related to CO_2 solubility, and this term can be used to describe the compression at great pressures.

3.3. Adsorption and Swelling. Figure 8 demonstrates that the swelling of specimens decreases linearly by 1.5% with the increase of adsorption amount by 1 mmol/g, which is shown in the previous study [13]. Studies reported an increase in deformation with the augment of absolute adsorption, along with a stable trend at CO_2 pressures approaching 10 MPa [15, 29]. The process of CO_2 adsorption and specimen deformation is from the disequilibrium state to the dynamic equilibrium state. With CO_2 injection, CO_2 diffuses due to pressure differences and it is absorbed by the matrix. CO_2 acts as the

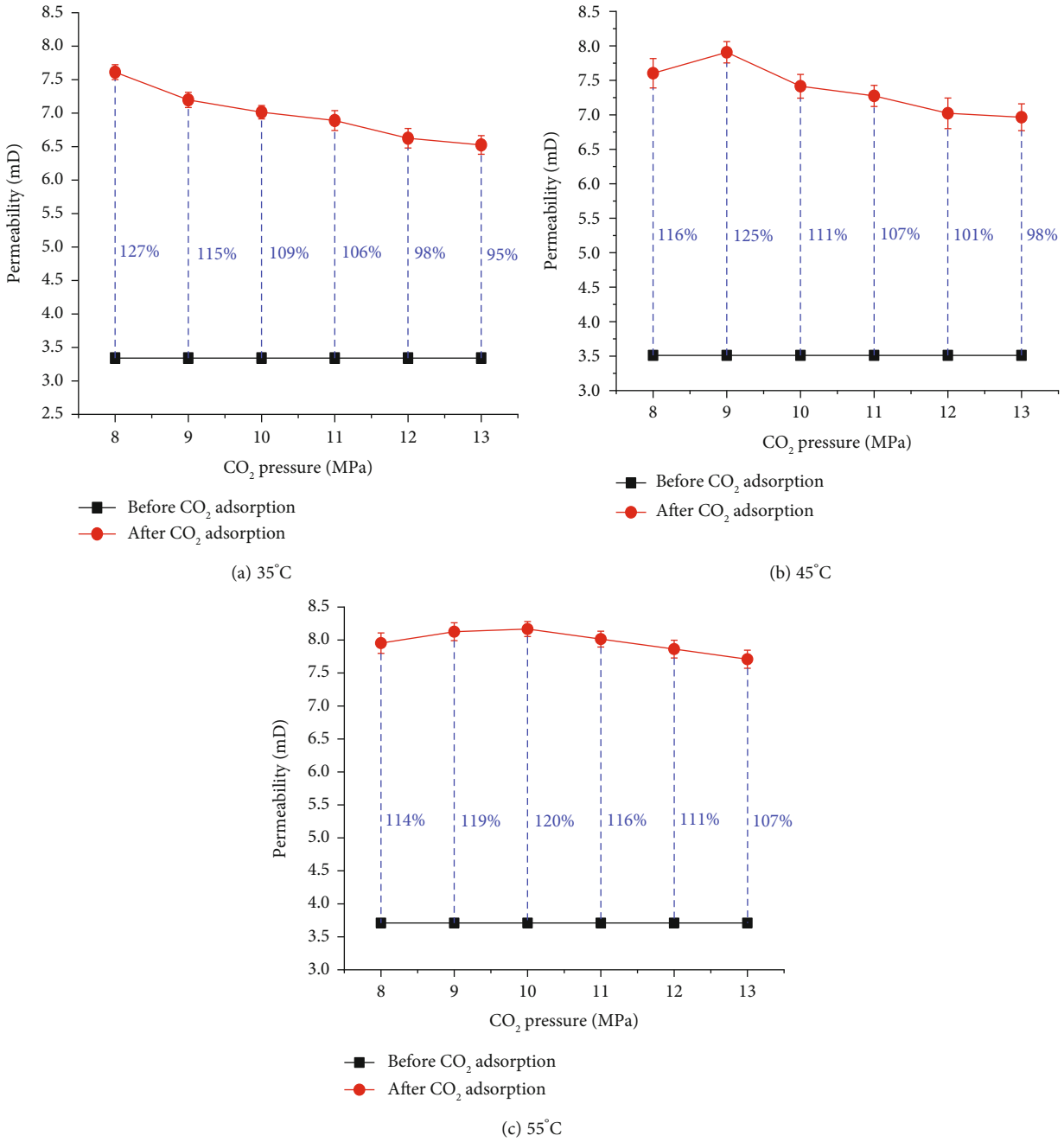

Figure 3: Permeability enhancement at different temperatures.

plasticizer and enables coal structure rearrangement, reducing the softening temperatures [30]. CO_2 adsorption can reduce the surface energy of the coal and weak mechanical properties. These are the main reasons that matrix swells significantly after adsorption. High-pressure CO_2 can constrain matrix swelling and the expansion shows a downward trend when CO_2 pressures exceed 10 MPa.

3.4. Analysis of the Permeability Changes Induced by CO_2. The permeability ratio shows a linear augment with the volumetric swelling as shown in Figure 9. It is noted that the proportion at 55°C is slightly lower than that at other temperatures. The adsorption-induced swelling indicates greater porosity and wider seepage channels, and therefore, permeability is enhanced. This reveals that the permeability enhancement under nonconfinement is influenced mostly by the adsorption.

For CO_2 geological storage in deep coal seams, where strata pressures restrict the swelling, the permeability variation after CO_2 interaction is a coupled result of CO_2 adsorption and effective stresses, along with extraction or dissolution. For CO_2 adsorption in the confined stress, due to gas injection, both the reduction in effective stresses and CO_2 adsorption induce matrix expansion (equations (6) and (7)). Under the

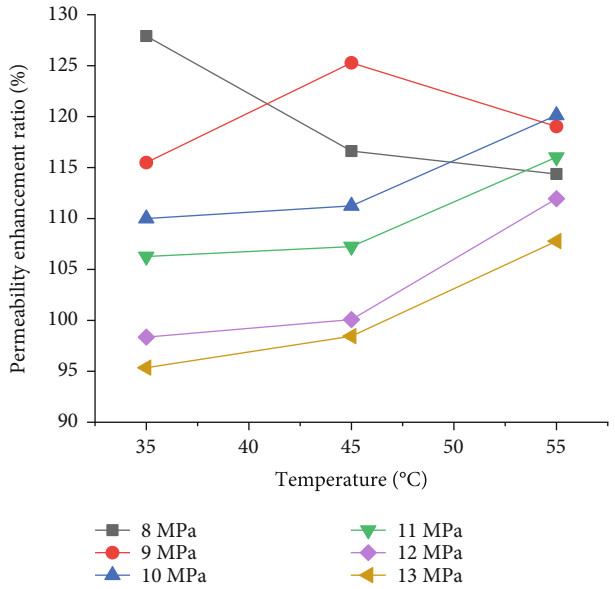

Figure 4: Permeability enhancement ratio with the increase of temperatures.

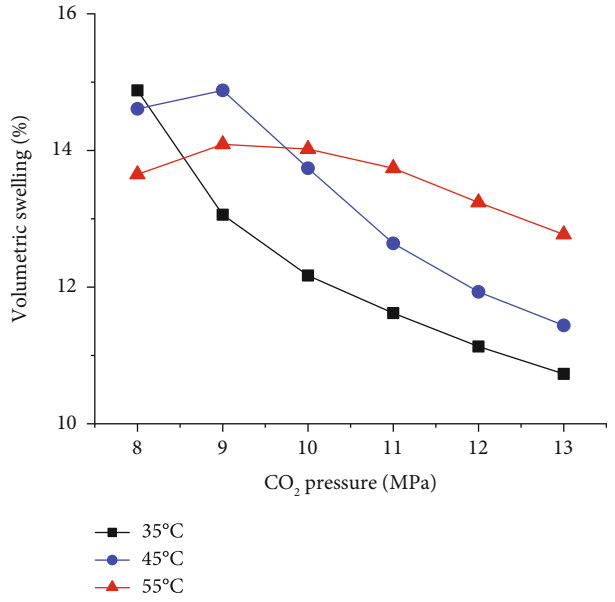

Figure 5: Volumetric swelling at different pressures and temperatures.

great confinement, the coal matrix expands inward and cleats narrow, leading to permeability reduction. Ranathunga et al. observed shrinkage in macropores with the help of scanning electron microscopy (SEM) [31]. All microcleats, the main channels of gas seepage, can be observed closely by micro-CT scanning after SC-CO_2 injection, and permeability decreases drastically by 2 orders of magnitude [32]. After CO_2 adsorption under a constraint pressure, the permeability reduction ratio augments linearly with the increase of swelling [33].

$$\varepsilon = \varepsilon_e + S, \tag{6}$$

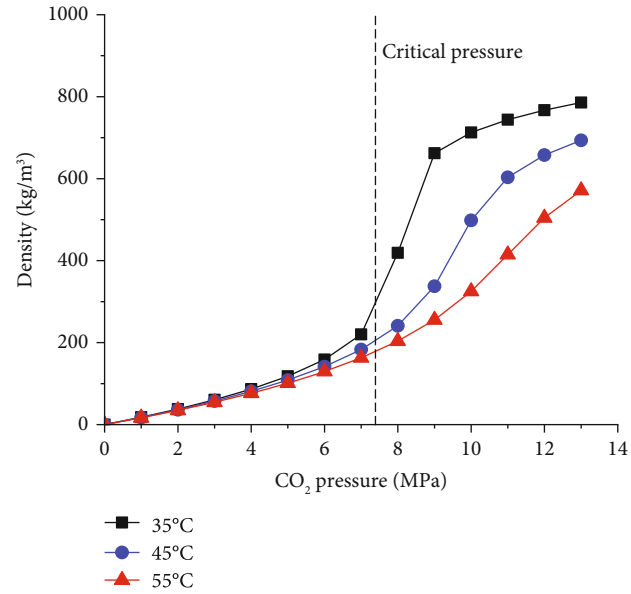

Figure 6: CO_2 density at different temperatures and pressures.

$$\varepsilon_e = -\frac{\sigma - P}{3K}, \tag{7}$$

where ε is the total deformation induced by effective stresses and adsorption. ε_e is the volumetric deformation caused by effective stresses, namely, $\sigma - P$, and K is the bulk modulus. In equation (7), the minus indicates compression.

As a solvent, SC-CO_2 can extract organic minerals and alter the pore surface, tarnishing the surface. Li et al. observed permeability augment after CO_2 cycling adsorption and desorption under a constraint pressure, along with the expansion in macro- and mesopores but few changes in micropores [34]. Because of noticeable fractures on the surface, the extraction is attributed to the remarkable permeability improvement. The solubility varies with CO_2 density, and therefore, it is difficult to quantify the effects of extraction.

Another influencing factor is the chemical reaction. Water exists in coal seams, and the interaction of CO_2 and water can dissolve the carbonate minerals. CO_2 could dissolve in water forming an acid solution, in which calcite is dissolved. The interaction of water and SC-CO_2 causes an increment in pores, and the permeability is improved [23]. Nevertheless, some silicate minerals could form precipitation and block pore connections, reducing the permeability [22].

3.5. Discussion for CO_2-ECBM. CO_2-ECBM is injecting CO_2 through wells into deep coal seams at a certain injection pressure. The permeability is the key factor during gas production. Although the permeability becomes greater at high pressures without considering the Klinkenberg effect [7], however, increasing CO_2 pressures cannot be effective for improving exploitation efficiency according to the previous analysis. Among the four factors, the effect of extraction and solution on permeability is limited and estimated difficultly. Swelling decreases gradually with the increase of CO_2 pressure. Besides, injecting high-pressure CO_2 is liable

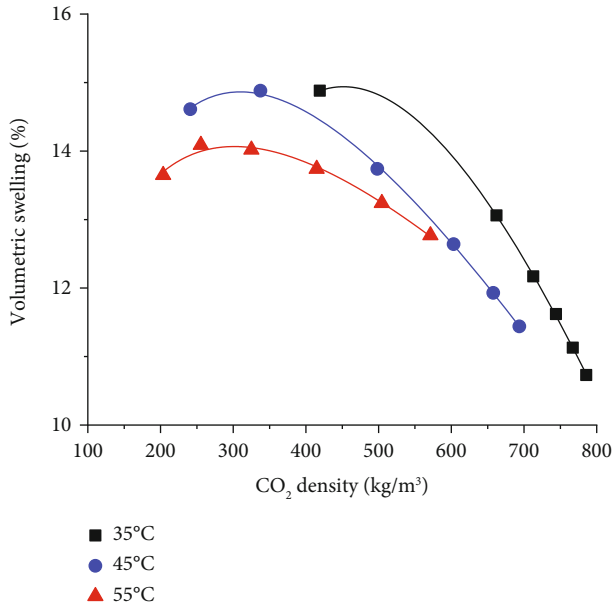

Figure 7: Expansion fits with CO_2 densities.

Table 1: Fitting parameters for the modified D-R model.

Temperature (°C)	S_{max}	D	a
35	0.32	0.28	-2.7×10^{-4}
45	0.23	0.11	-1.6×10^{-4}
55	0.19	0.07	-1.1×10^{-4}

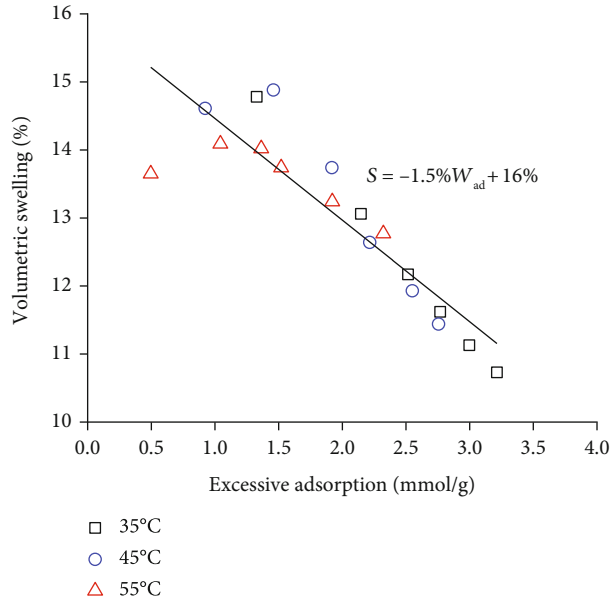

Figure 8: Volumetric swelling with excessive adsorption.

to induce disasters and weaken the mechanical properties. Therefore, the permeability could be not enhanced significantly by only increasing CO_2 pressures.

According to the national standard, numerous adsorption experiments last for 24 hours, after which the surface area decreases, while the surface area augments remarkably after 7 days and 14 days [21]. Kutchko et al. summarized no significant variations in macropores after 104 days considering the offset [35]. Due to limited observation, SEM images cannot reflect total surface changes, while those changes can be estimated in other methods such as CT and nuclear magnetic resonance (NMR) [36, 37]. The interaction time should be taken into consideration, and further studies are required to investigate the long-term changes and mechanical behavior for coal of different ranks.

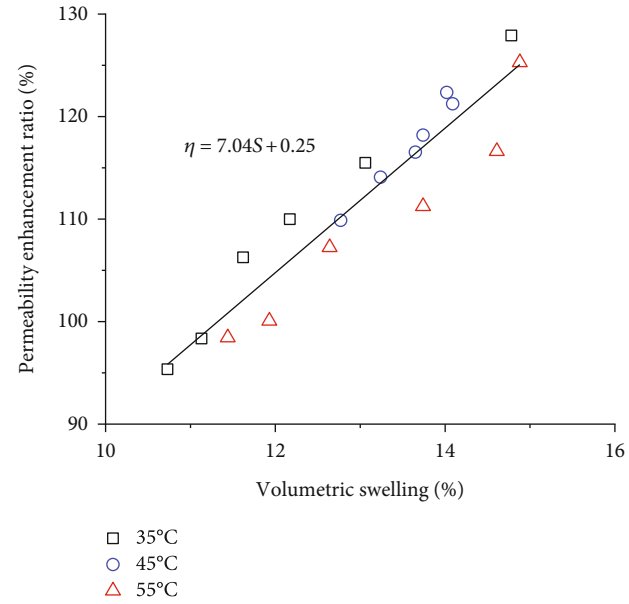

Figure 9: Permeability enhancement ratio with volumetric swelling.

4. Conclusions

Permeability characteristics were investigated on briquettes before and after SC-CO_2 adsorption under nonconfinement. The main results are as follows:

(1) Permeability enhances significantly after CO_2 adsorption in briquettes. The permeability enhancement reduces continuously with the increase of CO_2 pressure at 35°C, while it augments slightly before decreasing moderately at 45 and 55°C

(2) CO_2 adsorption could cause volumetric swelling, and expansion is fitted well with the modified D-R model at the considering temperatures

(3) The permeability enhancement ratio is a linear function with swelling. The permeability enhancement under nonconfinement is influenced mainly by SC-CO_2 adsorption

(4) For CO_2 storage in coal seams, the permeability is influenced by four factors, effective stresses, dsorption, extraction, and solution, and the limited effects of extraction and solution are difficult to quantify. Further research is required to study long-term variations in permeability and mechanical properties

Notations

k: Permeability, mD
μ: Viscosity, μPa•s
Q: Flow rate, cm^3/s
P_1: Upstream pressure, MPa
P_2: Downstream pressure, MPa
L: Length, cm
A: Cross-sectional area, cm^2
S: Volumetric expansion
V: Initial volume of the specimen, cm^3
V_0: Final volume of the specimen, cm^3
n: Adsorption amount per unit of a specimen, mol/g
m: Weight, g
T: Equilibrium temperature, K
V_R: Volume of the reference cell, cm^3
P_{R1}: Initial pressure of the reference cell, MPa
P_{R2}: of the reference cell, MPa
Z_{R1}: Compressibility factor corresponding to P_{R1}
Z_{R2}: Compressibility factor corresponding to P_{R2}
V_{A1}: Initial void volume of the adsorption cell, cm^3
V_{A2}: Final void volume of the adsorption cell, cm^3
P_{A1}: Initial pressure of adsorption cell, MPa
P_{A2}: Final presures of adsorption cell, MPa
Z_{A1}: Compressibility factor corresponding to P_{A1}
Z_{A2}: Compressibility factor corresponding to P_{A2}
η: Permeability enhancement ratio
k_0: Permeability before CO_2 adsorption, mD
S_{max}: Maximum swelling
D: Empirical parameter
ρ_a: density of adsorbed CO_2, kg/m^3
ρ: CO_2 density, kg/m^3
a: Empirical parameter
ε: Total deformation of a specimen
ε_e: Volumetric deformation caused by effective stresses
σ: Volume stress, MPa
P: Pore pressure, MPa
K: Bulk modulus, MPa.

Data Availability

The data used to support the findings of this study are available from the corresponding author upon request.

Conflicts of Interest

The authors declare that there is no conflict of interest regarding the publication of this paper.

Acknowledgments

This study was supported by the National Natural Science Foundation of China (No. 51874144 and No. 51679093) and Scientific and Technology Plan Projects in Xiamen (No. 3502z20193040).

References

[1] R. S. Haszeldine, "Carbon capture and storage: how green can black be?," *Science*, vol. 325, no. 5948, pp. 1647–1652, 2009.

[2] J. Yun, F. Xu, L. Liu, N. Zhong, and X. Wu, "New progress and future prospects of CBM exploration and development in China," *International Journal of Mining Science and Technology*, vol. 22, no. 3, pp. 363–369, 2012.

[3] S. R. Reeves, "The Coal-Seq project: key results from field, laboratory, and modeling studies," in *Greenhouse Gas Control Technologies 7*, pp. 1399–1403, Elsevier, 2005.

[4] J. Q. Shi, S. Durucan, and M. Fujioka, "A reservoir simulation study of CO_2 injection and N_2 flooding at the Ishikari coalfield CO_2 storage pilot project, Japan," *International Journal of Greenhouse Gas Control*, vol. 2, no. 1, pp. 47–57, 2008.

[5] J. Ye, S. Feng, Z. Fan et al., "Micro-pilot test for enhanced coalbed methane recovery by injecting carbon dioxide in south part of Qinshui Basin," *Acta Petrolei Sinica*, vol. 28, no. 4, pp. 77–80, 2007.

[6] R. Span and W. Wagner, "A new equation of state for carbon dioxide covering the fluid region from the triple-point temperature to 1100 K at pressures up to 800 MPa," *Journal of Physical and Chemical Reference Data*, vol. 25, no. 6, pp. 1509–1596, 1996.

[7] D. Wu, X. Liu, B. Liang, K. Sun, and X. Xiao, "Experiments on displacing methane in coal by injecting supercritical carbon dioxide," *Energy & Fuels*, vol. 32, no. 12, pp. 12766–12771, 2018.

[8] V. Vishal, T. N. Singh, and P. G. Ranjith, "Influence of sorption time in CO_2 -ECBM process in Indian coals using coupled numerical simulation," *Fuel*, vol. 139, pp. 51–58, 2015.

[9] V. Vishal, B. Mahanta, S. P. Pradhan, T. N. Singh, and P. G. Ranjith, "Simulation of CO_2 enhanced coalbed methane recovery in Jharia coalfields, India," *Energy*, vol. 159, pp. 1185–1194, 2018.

[10] Y. Fan, C. Deng, X. Zhang, F. Li, X. Wang, and L. Qiao, "Numerical study of CO_2-enhanced coalbed methane recovery," *International Journal of Greenhouse Gas Control*, vol. 76, pp. 12–23, 2018.

[11] S. Harpalani and R. A. Schraufnagel, "Shrinkage of coal matrix with release of gas and its impact on permeability of coal," *Fuel*, vol. 69, no. 5, pp. 551–556, 1990.

[12] R. Wang, Q. Wang, Q. Niu, J. Pan, H. Wang, and Z. Wang, "CO_2 adsorption and swelling of coal under constrained conditions and their stage-change relationship," *Journal of Natural Gas Science and Engineering*, vol. 76, p. 103205, 2020.

[13] D. Wu, X. Liu, K. Sun, X. Xiao, and L. Xin, "Experiments on supercritical CO_2 adsorption in briquettes," *Energy Sources, Part A: Recovery, Utilization, and Environmental Effects*, vol. 41, no. 8, pp. 1005–1011, 2018.

[14] H. Liu, S. Sang, S. Liu et al., "Supercritical-CO_2 adsorption quantification and modeling for a deep coalbed methane reservoir in the southern Qinshui Basin, China," *ACS Omega*, vol. 4, no. 7, pp. 11685–11700, 2019.

[15] J. Jia, S. Sang, L. Cao, and S. Liu, "Characteristics of CO_2/supercritical CO_2 adsorption-induced swelling to anthracite: an experimental study," *Fuel*, vol. 216, pp. 639–647, 2018.

[16] H. Liu, B. Lin, and W. Yang, "Theoretical models for gas adsorption-induced coal deformation under coal seam field conditions," *Energy Science & Engineering*, vol. 7, no. 5, pp. 1504–1513, 2019.

[17] K. Zhang, Y. Cheng, K. Jin et al., "Effects of supercritical CO_2 fluids on pore morphology of coal: implications for CO_2 geological sequestration," *Energy & Fuels*, vol. 31, no. 5, pp. 4731–4741, 2017.

[18] K. Zhang, Y. Cheng, W. Li, D. Wu, and Z. Liu, "Influence of supercritical CO_2 on pore structure and functional groups of coal: implications for CO_2 sequestration," *Journal of Natural Gas Science and Engineering*, vol. 40, pp. 288–298, 2017.

[19] M. A. Pirzada, M. Zoorabadi, H. Lamei Ramandi, I. Canbulat, and H. Roshan, "CO_2 sorption induced damage in coals in unconfined and confined stress states: a micrometer to core scale investigation," *International Journal of Coal Geology*, vol. 198, pp. 167–176, 2018.

[20] M. S. A. Perera and K. H. S. M. Sampath, "Modelling of free and adsorbed CO_2-induced mechanical property alterations in coal," *International Journal of Coal Geology*, vol. 217, p. 103348, 2020.

[21] K. H. S. M. Sampath, I. Sin, M. S. A. Perera, S. K. Matthai, P. G. Ranjith, and L. Dong-yin, "Effect of supercritical-CO_2 interaction time on the alterations in coal pore structure," *Journal of Natural Gas Science and Engineering*, vol. 76, p. 103214, 2020.

[22] X. Ni, Q. Li, Y. Wang, and S. Gao, "Permeability variation characteristics of coal after injecting carbon dioxide into a coal seam," *International Journal of Mining Science and Technology*, vol. 25, no. 4, pp. 665–670, 2015.

[23] C. Liu, S. Sang, X. Fan et al., "Influences of pressures and temperatures on pore structures of different rank coals during CO_2 geological storage process," *Fuel*, vol. 259, p. 116273, 2020.

[24] J. Yu, X. Chen, H. Li, J. Zhou, and Y. Cai, "Effect of freeze-thaw cycles on mechanical properties and permeability of red sandstone under triaxial compression," *Journal of Mountain Science*, vol. 12, no. 1, pp. 218–231, 2015.

[25] J. Yu, X. Chen, Y. Cai, and H. Li, "Triaxial test research on mechanical properties and permeability of sandstone with a single joint filled with gypsum," *KSCE Journal of Civil Engineering*, vol. 20, no. 6, pp. 2243–2252, 2016.

[26] J. Yu, W. Yao, K. Duan, X. Liu, and Y. Zhu, "Experimental study and discrete element method modeling of compression and permeability behaviors of weakly anisotropic sandstones," *International Journal of Rock Mechanics and Mining Sciences*, vol. 134, p. 104437, 2020.

[27] J. Yu, S. Chen, X. Chen, Y. Zhang, and Y. Cai, "Experimental investigation on mechanical properties and permeability evolution of red sandstone after heat treatments," *Journal of Zhejiang University-SCIENCE A*, vol. 16, no. 9, pp. 749–759, 2015.

[28] R. Sakurovs, S. Day, S. Weir, and G. Duffy, "Application of a modified Dubinin- Radushkevich equation to adsorption of gases by coals under supercritical conditions," *Energy & Fuels*, vol. 21, no. 2, pp. 992–997, 2007.

[29] S. Day, R. Fry, and R. Sakurovs, "Swelling of Australian coals in supercritical CO_2," *International Journal of Coal Geology*, vol. 74, no. 1, pp. 41–52, 2008.

[30] J. W. Larsen, "The effects of dissolved CO_2 on coal structure and properties," *International Journal of Coal Geology*, vol. 57, no. 1, pp. 63–70, 2004.

[31] A. S. Ranathunga, M. S. A. Perera, P. G. Ranjith, and H. Bui, "Super-critical CO_2 saturation-induced mechanical property alterations in low rank coal: an experimental study," *The Journal of Supercritical Fluids*, vol. 109, pp. 134–140, 2016.

[32] Y. Zhang, M. Lebedev, M. Sarmadivaleh, A. Barifcani, and S. Iglauer, "Swelling-induced changes in coal microstructure due to supercritical CO_2 injection," *Geophysical Research Letters*, vol. 43, no. 17, pp. 9077–9083, 2016.

[33] Q. Niu, L. Cao, S. Sang, X. Zhou, and S. Liu, "Experimental study of permeability changes and its influencing factors with CO_2 injection in coal," *Journal of Natural Gas Science and Engineering*, vol. 61, pp. 215–225, 2019.

[34] W. Li, Z. Liu, E. Su, and Y. Cheng, "Experimental investigation on the effects of supercritical carbon dioxide on coal permeability: implication for CO_2 injection method," *Energy & Fuels*, vol. 33, no. 1, pp. 503–512, 2018.

[35] B. G. Kutchko, A. L. Goodman, E. Rosenbaum, S. Natesakhawat, and K. Wagner, "Characterization of coal before and after supercritical CO_2 exposure via feature relocation using field-emission scanning electron microscopy," *Fuel*, vol. 107, pp. 777–786, 2013.

[36] B. Mahanta, P. G. Ranjith, T. N. Singh, V. Vishal, W. Duan, and M. Sazid, "Digital rock physics and application of high-resolution micro- CT techniques for geomaterials," in *Deep Rock Mechanics: From Research to Engineering*pp. 299–307, Taylor Francis Group, London.

[37] Y. Cai, J. Yu, G. Fu, and H. Li, "Experimental investigation on the relevance of mechanical properties and porosity of sandstone after hydrochemical erosion," *Journal of Mountain Science*, vol. 13, no. 11, pp. 2053–2068, 2016.